ACS APPLIED MATERIALS & INTERFACES

Research Article

www.acsami.org

Polyamine-Mediated Interfacial Assembly of rGO-ZnO Nanostructures: A Bio-inspired Approach and Enhanced Photocatalytic Properties

Thuniki Naveen Reddy,[†,‡] Joydeb Manna,[†] and Rohit K. Rana*[,†,‡]

[†]Nanomaterials Laboratory, Inorganic and Physical Chemistry Division, and [‡]Academy of Scientific and Innovative Research, CSIR-Indian Institute of Chemical Technology, Hyderabad 500 007, India

Supporting Information

ABSTRACT: A bio-inspired approach for the fabrication of reduced graphene oxide (rGO) embedded ZnO nanostructure has been attempted to address issues pertaining to charge recombination and photocorrosion in ZnO for application as an effective photocatalyst. Herein we demonstrate the synthesis of rGO-ZnO nanostructures in a single step using polyamines, which simultaneously aid in the mineralization of ZnO nanostructures from zinc nitrate, reduction of graphene oxide (GO), and finally their assembly to form rGO-ZnO composite structures under environmentally benign conditions. The interspersed nanocomponents in the assembled heterostructures result in enhanced photocatalytic activity under UV light, indicating an effective charge separation of the excited electrons. Furthermore, the composite structure provides stability against photocorrosion for efficient recyclability of the catalyst.

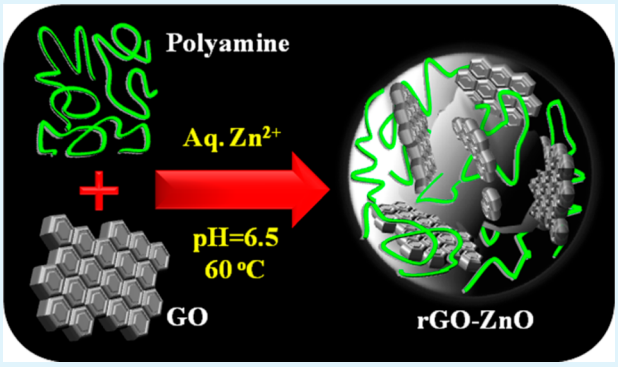

KEYWORDS: *bio-inspired mineralization, polyamine, zinc oxide, graphene, photocatalysis*

INTRODUCTION

ZnO based photoactive materials are of great interest because of their potential for addressing the environmental issues such as photodegrdation of organic parpollutants and conversion of photon into chemical energy.[1,2] However, the rapid recombination of photogenerated electron−hole pairs within the semiconductor material results in its low efficiency, thus limiting its practical applications. Several approaches have been reported for effective charge separation such as by combining with metal nanoparticles[3,4] or with other semiconductor materials.[5,6] The role in the heterostructure is to drain or trap photoexcited electrons and thereby separate the electron−hole pairs. Particularly, a lot of attention has recently been paid to the carbon−semiconductor hybrid materials having potential for improved photoactivity via their effectiveness in electron-trapping.[7]

In this context, graphene, a two-dimensional allotrope of carbon, has been proven to enhance the photocatalytic activity of various semiconductors including ZnO.[8,9] The combination of graphene has also been claimed to address the photocorrosion issues in ZnO.[7,10] Hence, there have been efforts to develop methodologies for the fabrication of nanostructured ZnO/graphene with properties suitable for photoinduced applications. Various methods, such as *in situ* photoreduction of graphene oxide on presynthesized ZnO,[11,12] solvothermal growth of ZnO on graphene sheets,[13−15] thermal decomposition of precursors,[16,17] colloidal mixing,[18] microwave method,[19] and ultrasonication,[20] etc., have been reported. However, these methods mostly require drastic conditions of either high temperature or strong alkali medium, while in some cases complicated multiple steps of fabrication processes are involved. The enhancement in photocatalytic activity is also dependent on the intrinsic differences in electron transportation and trapping capability of the graphene-ZnO in the composite structure, as well as their ability to absorb organic pollutants. So, there is a requirement to develop methodology for fabrication of such composite materials not only under environmentally benign conditions but also with improvement in the desired properties for photocatalytic applications.

In the present work, we make use of a bio-inspired route for assembly of ZnO and graphene to develop facile methodologies and to enhance interfacial interaction for improved photoactivities. Similar to the bio-mineralization processes, which occur in aqueous solution under ambient conditions of near neutral pH and room temperature, there have been efforts to develop methods for fabrication of functional materials.[21] Particularly in diatoms, it has been established that, in the bio-mineralization process, complex architecture is achieved via polyamine-mediated mineralization and assembly.[22] In this regard, our approach has been to explore and develop

Received: June 2, 2015
Accepted: August 19, 2015
Published: August 19, 2015

DOI: 10.1021/acsami.5b04820
ACS Appl. Mater. Interfaces 2015, 7, 19684−19690

polyamine-mediated bio-inspired methods for fabrication of nanostructured materials with control on size and morphology under environmentally benign conditions.[23−25] Herein we demonstrate that poly(allylamine), which can mineralize ZnO from water-soluble zinc precursor, simultaneously facilitates reduction of graphene oxide and their assembly to generate rGO-ZnO nanocomposites in a single step.

RESULTS AND DISCUSSION

The bio-inspired route to fabricate rGO-ZnO composites is schematically illustrated in Scheme 1. First to examine the

Scheme 1. Schematic Representation of the Polyamine-Mediated Bio-inspired Mineralization of ZnO in the Presence of GO Leading to the Formation of rGO-ZnO Assembled Structure

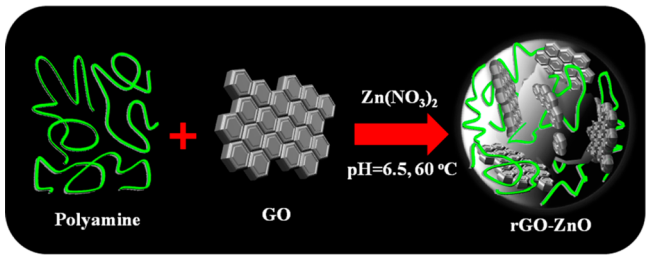

interaction of GO with polyamine, we mixed an aqueous suspension of graphene oxide (GO) with poly(allylamine). It resulted in stabilization of the suspension as indicated by dynamic light scattering (DLS) analysis. From the ζ potential measurements we observed that the initially negatively charged GO particles became positively charged with their interaction with the polyamines. This suggested a successful functionalization of the GO with the polyamine via the interactions among (-C−OH, -C═O, and -COOH, etc.) and amine groups.[26,27] The polyamines, which are also known to be responsible for bio-mineralization processes,[22−25] were then utilized for mineralization of ZnO in the presence of GO so that the poly(allylamine), while mineralizing ZnO, can simultaneously functionalize GO under the mild conditions at 60 °C and neutral pH in an aqueous medium. As shown in Scheme 1, addition of poly(allylamine) into a mixture containing zinc nitrate and graphene oxide resulted in an immediate gray color precipitate (rGO-ZnO), which was collected for further analyses (Supporting Information (SI) Table S1).

Figure 1 shows the XRD patterns of the synthesized rGO-ZnO and ZnO along with that of graphite and GO for comparison. The XRD pattern of graphite in Figure 1a shows a typical diffraction peak at 2θ = 26.4° representing the graphitic layers. In the case of GO, while the graphitic peak disappeared, a new diffraction peak appeared at 2θ = 12.6°. Clearly with oxidation of graphite the interlayer distance increased from graphite (0.335 nm) to graphene oxide (0.672 nm). This is indicative of hydration and exfoliation of GO in an aqueous medium facilitated via formation of various oxygen containing functionalities, such as hydroxyl, epoxy, carbonyl, and carboxyl groups, etc.[16,27] Further it was observed that, in the as-synthesized rGO-ZnO, the characteristic diffraction peak of GO disappeared and instead a broad peak appeared at 2θ = 22.4° (Figure 1b). This suggests that the crystallographic ordering has been lost leading to a random packing of the graphene sheets in rGO.[16,27] In addition, the mineralized ZnO exhibited

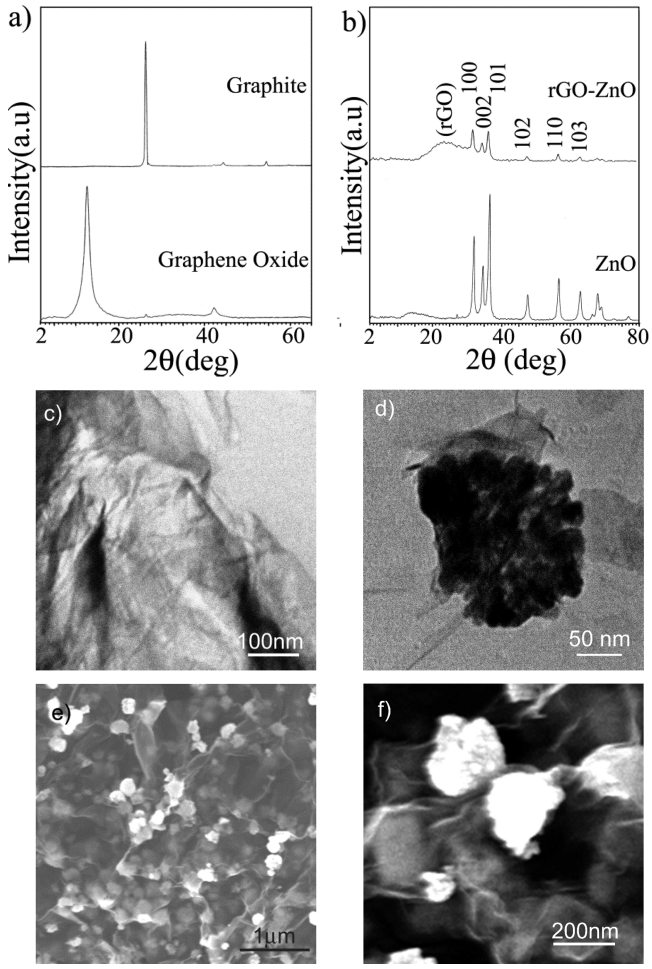

Figure 1. X-ray diffraction patterns of (a) graphite flakes and GO and (b) ZnO and rGO-ZnO; transmission electron microscopy (TEM) images of the synthesized (c) GO and (d) rGO-ZnO; and (e, f) field emission scanning electron microscopy (FE-SEM) images of rGO-ZnO at different magnifications.

XRD peaks assignable to (100), (002), (110), (102), and (103) planes of a wurzite phase (JCPDS card no. 36-1451).[25] The crystallite size of ZnO as estimated using the Debye−Scherrer equation was ∼8 nm, while the ZnO prepared in the absence of GO had a crystallite size of ∼14.5 nm. Therefore, we believe that the presence of graphene sheets during the ZnO mineralization restricts the growth of the mineralized crystallites by stabilizing the smaller crystallites on their surface.

The transmission electron microscopy (TEM) images of graphene oxide sheets and rGO-ZnO are shown in Figure 1c,d. The TEM image illustrates the exfoliated graphene oxide sheets. In the rGO-ZnO, the mineralized ZnO particles are seen entangled with the rGO sheets to form nearly spherical aggregates (Figure 1d). Further examination reveals that the ZnO particles are of ∼20−25 nm sizes as assembled in the aggregate. The selected area electron diffraction (SAED) of graphene oxide (SI Figure S1) showed ring patterns assignable to (1100) and (1120) planes of a hexagonal crystal lattice.[28] In the case of rGO-ZnO, there were additional spots in the SAED pattern due to the wurzite phase of ZnO in conformity with the XRD result. The scanning electron microscopy (SEM) analysis indicated the sheet-like morphology of the GO (SI Figure S2a). In the SEM image of rGO-ZnO, we observed the presence of spherical aggregates of sizes 180−220 nm (Figure 1e). The

DOI: 10.1021/acsami.5b04820
ACS Appl. Mater. Interfaces 2015, 7, 19684−19690

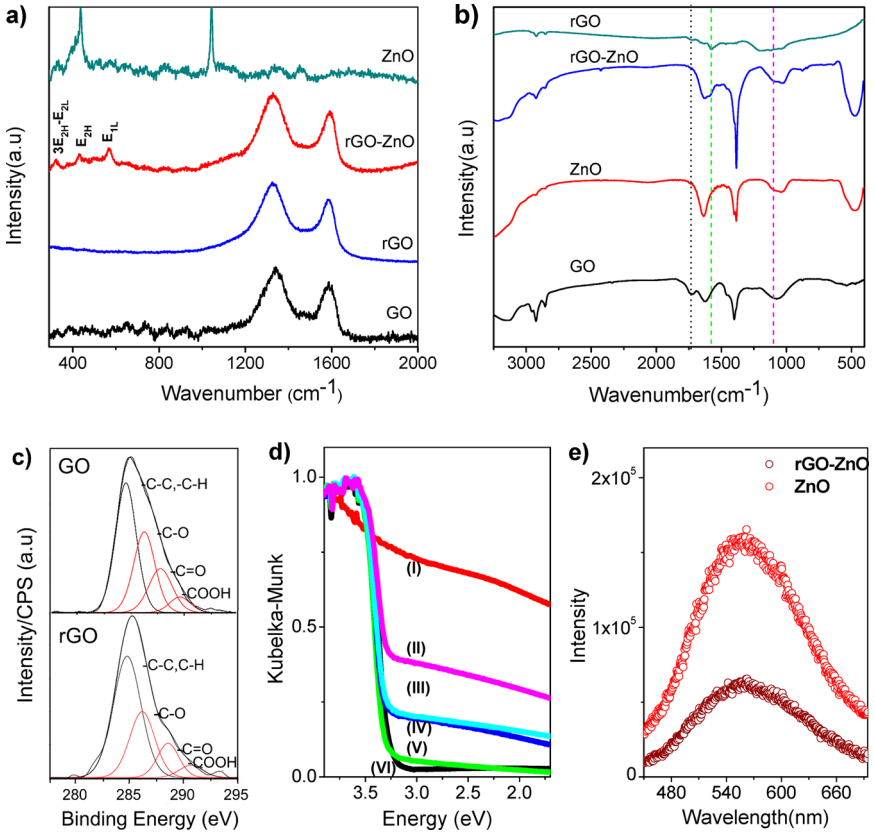

Figure 2. (a) Confocal micro-Raman and (b) FT-IR spectra of the as-synthesized samples; (c) XPS spectra for C 1s; (d) UV-DRS spectra of (i) rGO and (ii–vi) rGO-ZnO with rGO wt % of (ii) 2.26, (iii) 2.07, (iv) 1.78, (v) 1.60, and (vi) ZnO; and (e) emission spectra of rGO-ZnO and ZnO keeping the ZnO amount constant.

particles were slightly smaller than the sizes seen for the ZnO sample (SI Figure S2b). Further analysis by field emission SEM (FE-SEM) revealed that the assembly of graphene sheets along with the mineralized ZnO nanoparticles generated the spherical structures (Figure 1f). As shown earlier, the polyamine facilitates both the mineralization and assembly of ZnO nanoparticles under mild conditions.[24] In the present case, when we carried out the reaction in the absence of polyamine, there was no ZnO formation. It also indicates that the GO does not have any influence on the mineralization process.

The DLS analysis of rGO-ZnO showed a hydrodynamic size distribution in the range of 100–250 nm (SI Figure S3). On the other hand, the ZnO particles prepared in the absence of GO had a broader size distribution of 110–520 nm. This suggests that the presence of GO not only restricts the growth of the crystallite size of ZnO as estimated from XRD but also influences the assembly process to narrow down the size distribution of the aggregates. ζ potential measurement showed that the ZnO particles mineralized in the absence of GO had a ζ potential of 46.4 mV (SI Figure S4). In the case of rGO-ZnO, the electrostatic interaction of amine groups in polyamine with GO besides ZnO led to a decrease in the ζ potential to 33.8 mV. It is also plausible that since this additional interaction of polyamine with GO can result in a lesser number of amine groups being available for the mineralization of ZnO, it may produce a lesser number of ZnO nanoparticles and hence generate smaller sized aggregates as seen in rGO-ZnO compared with that in ZnO.

The confocal micro-Raman analysis was carried out to identify the different forms of carbon present in the prepared materials (Figure 2a). In the case of both rGO-ZnO and GO there were two typical Raman shifts at 1328 and 1589 cm^{-1} indicating the D band (disordered carbon) and the G band (sp^2 hybridized carbon), respectively. When the intensity ratio (I_D/I_G) was compared, interestingly it was found to increase from a value of 1.23 for GO to 1.39 for rGO-ZnO. This increase in I_D/I_G is a clear indication that the graphene oxide has been reduced in the rGO-ZnO sample, which results in new extended sp^2 domains that are smaller in size but in greater number than those present in GO before reduction.[16] Further, to understand the reduction process, we performed a control reaction in which the polyamine was reacted with GO in the absence of the zinc precursor under similar conditions. It was observed that the polyamine could reduce GO to rGO (Figure 2a) as evident from the corresponding increase in the I_D/I_G ratio to 1.32. On the other hand, when the preceding reaction was carried out without polyamine, the I_D/I_G ratio did not change much (1.25; SI Figure S5d). Similar reduction of GO by various organic reagents containing amine functionalities has also been observed previously.[29,30]

Additional Raman shifts at 325, 434, and 570 cm^{-1} observed in the case of ZnO and rGO-ZnO samples could be assigned to various vibrational modes ($3E_{2H}-E_{2L}$, E_{2H}, and E_{1L}) in ZnO.[25,31] When compared with the spectra of ZnO, the E_{1L} intensity in case of rGO-ZnO was found to be relatively higher. Since the E_{1L} mode signifies the presence of oxygen vacancies in the ZnO lattice, it further suggests that the rGO-ZnO has more lattice defects. These defects are generally attributed to homogeneously distributed surface impurities or the presence of dopants, which in our case may be due to the presence of

DOI: 10.1021/acsami.5b04820
ACS Appl. Mater. Interfaces 2015, 7, 19684–19690

polyamines and rGO attached with ZnO nanoparticles.[25] As has been shown previously, more interfacial contact between rGO and ZnO can lead to such surface defects and therefore can result in better photoactivity and anti-photocorrosion properties.[32] Moreover these vacant sites in ZnO, which act as anchor sites for the carbon based materials, can substantially reduce the activation of the surface oxygen atom resulting in photocorrosion inhibition of ZnO.[7]

The FT-IR spectra for ZnO and rGO-ZnO showed the characteristic Zn−O stretching band at 470 cm^{-1} (Figure 2b, SI Table S2). The bands at 1734 and 1074 cm^{-1} assignable to the stretching vibrations of C═O and C−O, respectively, indicated the presence oxygen containing functionalities in GO. The N−H vibration at 1630 cm^{-1} due the amine groups confirmed the presence of poly(allylamine) in the mineralized samples. After reduction of GO, we found a decrease in the intensity of the C═O and C−O stretching bands with a simultaneously increase in the intensity of 1563 cm^{-1} (C═C) and 874 cm^{-1} (aromatic OH) bands in the spectra of rGO-ZnO and rGO. The reduction of GO was further investigated by XPS. The XPS elemental survey of rGO-ZnO revealed the presence of Zn along with C (carbon) and O (oxygen) (SI Figure S6)). As estimated for GO, the C 1s to O 1s intensity ratio was 1.08, indicating the presence of oxygen containing species as a result of the oxidized graphitic layers. On further analysis the C 1s region revealed peaks at 284.9, 286.5, 287.9, and 289.8 eV, assignable to the carbon in C═C (C−H), C−OH, C═O, and COOH, respectively.[12] The presence of similar species was also observed in rGO-ZnO (Figure 2c). From the estimation of the peak areas of various carbon species, we observed a decrease in the amount of C−OH, C═O, and COOH in rGO-ZnO when compared with that in GO. The decrease was 8.3% for C−OH, 31.8% for C═O, and 33.3% for COOH, respectively (SI Table S3). Except for C−OH, for which the change in peak area was less due to the close proximity of the C 1s binding energy in C−OH and C−N (polyamine) bonds,[33] the decreases in C═O and COOH peaks were indicative of GO reduction. It further corroborated with the results obtained from Raman analyses confirming the presence of the reduced form of graphene oxide in rGO-ZnO.

The optical properties of the synthesized materials were characterized by using UV−vis diffuse reflectance spectroscopy (Figure 2d). The ZnO and rGO-ZnO samples showed an absorbance in the UV region (378 nm) corresponding to a band gap of 3.28 eV. The presence of reduced graphene oxide in rGO and rGO-ZnO was also supported by a corresponding increased absorption in the visible region. It was observed that with an increase in the weight percent of rGO in rGO-ZnO, the absorbance in the visible region increased. The fluorescence measurement showed a green emission at 562 nm, which was assigned to the lattice oxygen vacancies in ZnO. Quenching of this emission generally provides information regarding the interfacial electron transfer process between the excited ZnO and GO.[11] We observed that there was a decrease in the emission intensity by 62% in the case of rGO-ZnO as compared with ZnO when excited at 350 nm keeping the amount of ZnO the same (Figure 2e). In order to rule out any possibility of interference from the excitation of rGO, the absorption spectra were compared.[11] The fraction of light absorbed at 350 nm due to the presence of rGO in rGO-ZnO was 28.4% more than that of ZnO (SI Figure S7), which is less than the observed quenching in emission. Clearly it proves the interfacial electron transfer from the excited ZnO particles to rGO.

The photocatalytic activities of the rGO-ZnO samples were then tested to verify the effect of rGO in the composite structure. We carried out the photocatalytic reactions using rhodamine B (RhB) as the model pollutant under UV irradiation. For comparison, GO, rGO, and ZnO samples were also used as the catalysts under similar experimental conditions. It was observed that the combination of rGO with ZnO resulted in enhanced activity compared to that of only ZnO (Figure 3a and SI Figure S8). With rGO-ZnO (1.78 wt %

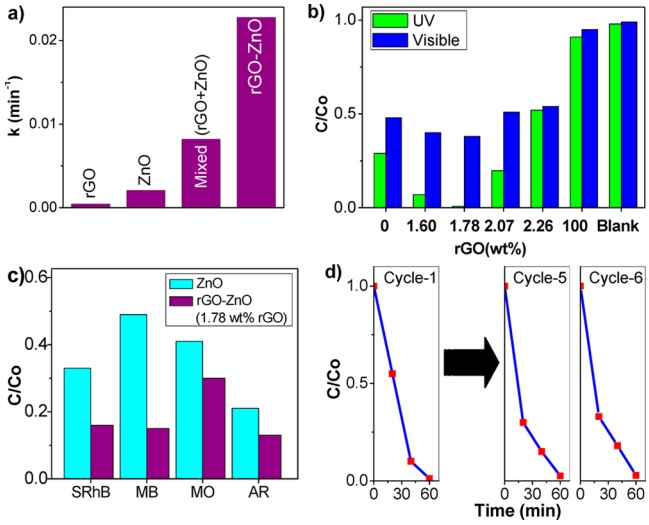

Figure 3. (a) Catalytic activity (k = apparent rate constant) of various catalysts in the RhB degradation under UV light; (b) activity of rGO-ZnO with different rGO content in the RhB degradation under visible and UV light; (c) photocatalytic degradation of various dyes (SRhB = sulforhodamine B, MB = methylene blue, MO = methyl orange, AR = alizarin red S) under UV light; and (d) activity of rGO-ZnO (1.78 wt % rGO) in various cycles for the degradation of RhB under UV-light.

rGO), 98.9% of the dye degraded under UV irradiation in 60 min. On the other hand, the ZnO sample showed 71.3% dye degradation under UV light. The enhanced activity in rGO-ZnO indicates that the presence of rGO facilitates the transfer of photoinduced electrons so as to prevent their recombination with the generated hole.[20] On the contrary, the material obtained by simply mixing the individual components (1.78 wt % polyamine-functionalized rGO and ZnO) prepared separately showed less activity than rGO-ZnO, indicating the importance of interfacial contact between ZnO and rGO toward the efficiency in photoactivity (Figure 3b). Therefore, we consider that the bio-inspired method wherein the *in situ* mineralization of ZnO takes place in the presence of GO, further enables better surface interactions among these components. The variation in rGO amount in rGO-ZnO showed an initial increase in the activity with the rGO content and then decreased with an optimum amount of rGO as low as 1.78 wt %. Photocatalytic activity of the catalyst for other dyes such as sulforhodamine B, alizarin red S, methylene blue, and methyl orange were also tested under UV light (Figure 3c). In all of the cases the enhancement of dye degradation was observed when rGO-ZnO was used as the catalyst.

For the photocatalytic reactions when carried out under visible light, it was observed that 61.5% of the dye was degraded within 60 min, while the ZnO showed 55.4% dye degradation and only rGO did not exhibit any substantial activity (Figure 3b). Although ZnO does not absorb in the visible region,

DOI: 10.1021/acsami.5b04820
ACS Appl. Mater. Interfaces 2015, 7, 19684−19690

introduction of a high level of surface defects or oxygen vacancies can enable visible-light-driven photocatalytic activity.[34] The high concentration of oxygen vacancies in ZnO has been suggested to be responsible for a narrowing of bandgap.[35] Since in our case there was not any apparent change in the ZnO absorbance, its activity under visible light can be attributed to the dye-sensitization mechanism (SI Figure S9).[36] So, the observed enhancement in activity for degradation of RhB under visible light was not as high as in the reaction under UV irradiation. Even with an increase in rGO content the change in activity was only marginal. Therefore, as suggested previously, the ZnO, when excited under UV light, can transfer its electron to graphene facilitated by the excellent electrical conductivity of the latter. On the other hand, the observed slight increase in activity under visible light could be due to the accompanied variation in surface area in rGO-ZnO (SI Table S4), which influences the amount of dye adsorbed on the catalyst (SI Figure S10 and Table S5).

The stability of the catalyst against photocorrosion is another important requirement for the applications of ZnO as photocatalysts. The reaction of the photogenerated holes with the surface oxygen on ZnO is the main reason for the decrease in activity. Therefore, a strong interaction between ZnO and rGO via formation of C−O linkages has been suggested to reduce the activation of the surface oxygen atom of ZnO and thereby can lead to the enhancement of photostability.[7] Photostability of the ZnO and rGO-ZnO was tested by performing recyclability experiments with RhB solution for different time intervals under UV irradiation. In the case of rGO-ZnO the catalytic activity was almost retained as tested up to a sixth cycle (Figure 3d) with a marginal decrease in activity by 2 wt % in cycles 5 and 6. On the other hand, the reused ZnO exhibited a clear decrease in activity by 15% as seen for the sixth cycle (SI Figures S11 and S12). The decrease in photocatalytic activity for ZnO resulted from the photocorrosion effect.[32] We therefore consider that the bio-inspired method to mineralize ZnO in the presence of GO leads to a composite structure of rGO-ZnO, that not only allows for enhanced photocatalytic activity but also effectively prevents the photocorrosion resulting in a stable catalyst with reusability.

CONCLUSIONS

In conclusion, a polyamine-mediated bio-inspired approach was shown to facilitate the preparation of rGO-ZnO under mild condition. The polyamine, while acting as a mineralizer for ZnO, further assisted in reduction of graphene oxide and assembly of these nanounits simultaneously to form a composite structure. This unique construction arises from the interactions of the polyamine with rGO and ZnO, allowing them to intersperse with each other for efficient interfacial interaction. As a result, enhanced photocatalytic activity was observed via effective separation of photoinduced carriers. Moreover, this interaction also provided photostability, allowing the catalyst to be recycled and reused without any loss in activity. Hence the bio-inspired method as demonstrated herein provides an effective route to fabricate hybrid structures as photocatalysts, which can further be extended for the preparation of other graphene−semiconductor based hybrid nanostructured materials having potential applications in various photoactive devices.

EXPERIMENTAL SECTION

Materials. Zinc nitrate hexahydrate ($Zn(NO_3)_2{\cdot}6H_2O$), poly(allylamine) (PAA, 17 kDa), potassium persulfate ($K_2S_2O_8$), $KMnO_4$, P_2O_5, graphite flakes (25 μm), rhodamine B (RhB), sulforhodamine B (SRhB), methylene blue (MB), methyl orange (MO), alizarin red S (AR), and dialysis sacks (12000 Da MWCO) were purchased from Sigma-Aldrich and used as received. In all cases, Millipore water (18.2 MΩ) was used for the solution preparation.

Synthesis of Graphene Oxide. Graphene oxide (GO) was synthesized by using modified Hummer's method.[37] Typically, 12 mL of H_2SO_4 and 1.5 g of graphite (25 μm) were mixed in a round-bottom (RB) flask. Then 1.25 g of P_2O_5 was added slowly, followed by the addition of 1.25 g of $K_2S_2O_8$ in a similar manner. After complete addition, the temperature of the solution mixture was slowly raised to 80 °C and kept static for 5 h. After the oxidation, the mixture was cooled to room temperature and slowly diluted with 0.25 L of water. The final mixture was then filtered and washed with 1.0 L of water and dried at 80 °C for 2 h. As such, preoxidized GO was then dissolved with 60 mL of H_2SO_4 in a RB flask and then the solution temperature was slowly lowered to 5 °C followed by slow addition of 7.5 g of $KMnO_4$. After the complete addition of $KMnO_4$, the temperature of the mixture was raised to 35 °C and stirred for 2 h. The solution was cooled to room temperature (RT) followed by slow addition of 0.25 L of water while keeping the RB flask in an ice bath. A 10 mL aliquot of H_2O_2 was then added slowly, and the solution was kept stirring for 4 h. The reaction mixture was centrifuged and washed with hot water for 8 times. The obtained dispersion was dialyzed with dialysis tubing for 2 days to remove residual ions. Thus, prepared GO was re-disperssed in water to get a final concentration of 2 mg/mL for further use.

Mineralization and Assembly of Zinc Oxide with Reduced Graphene Oxide (rGO-ZnO). Solid zinc nitrate was weighed and dissolved in 10 mL of GO in water in a RB flask to get a final Zn^{2+} concentration of 0.1 M. The solution temperature was then increased to 60 °C followed by drop by drop addition of 0.2 mL of PAA solution (100 mg/mL). A gray color precipitate formation was observed within 5 min. The reaction mixture was further stirred for about 12 h at a speed of 1500 rpm at the same temperature. Finally thus obtained product was centrifuged and washed 4 times with Millipore water and dried at RT. Synthesis of ZnO was carried out following the same method but in the absence of GO. SI Table S1 shows the variation in concentration of GO and the rGO to ZnO ratio in the final sample.

Photocatalytic Studies. For the photocatalytic reactions dye solutions were prepared by dissolving the required amount in deionized water (Millipore, 18.2 MΩ). All photocatalytic reactions were carried out using a 400 W Hg lamp as UV-light and a 400 W sodium vapor lamp as visible-light source. In a typical reaction, an aqueous suspension was prepared containing 0.5 mg/mL catalyst and 1×10^{-5} M dye solution. The mixture was sonicated for 10 min followed by stirring for 1 h in the dark in order to reach adsorption−desorption equilibrium for the dye on the catalyst. The reaction mixture was then kept in a photoreactor and irradiated with the light for various time durations. The reaction progress was monitored by measuring the amount of dye degraded at different time intervals. The catalyst was first separated by centrifugation, and then the amount of dye remaining in supernatant was estimated using a UV−vis spectrophotometer. The recycle experiment was carried out by collecting and washing the used catalyst and testing with fresh dye solution each time. The dye adsorption study on different samples was carried out by keeping the aqueous suspension containing 0.5 mg/mL catalyst and dye stirred in the dark for 1 h. The amount of dye adsorbed was calculated by using the following equation.

$$C_A = (C_O(1 - A_R/A_O))/B$$

where C_A = concentration of adsorbed dye, A_R = absorbance due to the residual dye after treatment with catalyst, C_O = initial concentration of dye, A_O = absorbance at C_O, and B = amount of catalyst.

The apparent rate constant k was determined by the first order rate expression:

DOI: 10.1021/acsami.5b04820
ACS Appl. Mater. Interfaces 2015, 7, 19684−19690

$$k = (\ln(A_O/A))/t$$

where A_O = absorbance of dye at time (t) of zero and A = absorbance of the dye at different time (t) intervals.

Characterization. Powder XRD patterns were recorded on a Siemens (Cheshire, U.K.) D5000 X-ray diffractometer using Cu Kα (λ = 1.5406 Å) radiation at 40 kV and 30 mA with a standard monochromator equipped with a Ni filter to avoid Cu Kβ interference. The powder XRD patterns were used to identify the crystalline phases of the precipitated powder and to estimate the crystallite size using the Debye–Scherrer formula [$L = 0.9\lambda/(D \cos \theta)$], where λ is the X-ray wavelength, θ is the Bragg angle, and D is the full width of the diffraction line (hkl) at half-maximum intensity (converted into radians). A transmission electron microscope (Philips Technai G2 FE1 F12), operating at 80–100 kV, was used to investigate the morphology and size of the particles. The samples for TEM were prepared by dispersing the material in ethanol by ultrasonication and drop-drying onto a Formvar-coated copper grid. SEM analyses were performed by using a Hitachi S-3000N scanning electron microscope operated at 10 kV, and FE-SEM analysis was performed on a JEOL-7610F instrument. FTIR spectra were recorded within 400–4000 cm^{-1} on a Bruker ALPHA spectrometer equipped with a DTGS detector. Confocal micro-Raman spectra were recorded on a Horiba Jobin-Yvon LabRam HR spectrometer using a 17 mW internal He–Ne laser source having a wavelength of 632.8 nm. N_2 physisorption measurements were performed with a Quantachrome NOVA4000e gas sorption system. ζ potential and particle size measurements were done using a Malvern Zetasizer (Nano-ZS) instrument equipped with the detector at 173° angle and with a 668 nm laser source. UV–vis absorbance was measured using a Varian Cary 5000 spectrometer. For the solid samples, the UV–vis spectra were recorded using a diffuse reflectance spectroscopy (DRS) accessory, and the absorbance was plotted using a Kubelka–Munk function. XPS analyses were carried out on a KRATOS AXIS 165 with a dual anode (Mg and Al) apparatus using the Mg Kα anode.

■ ASSOCIATED CONTENT

Supporting Information

The Supporting Information is available free of charge on the ACS Publications website at DOI: 10.1021/acsami.5b04820.

Experimental details giving microscopic images, structural, light scattering, ζ potential, and spectral data, surface areas, dye adsorption, ZnO recyclability, and benzoic acid degradation (PDF)

■ AUTHOR INFORMATION

Corresponding Author

*Fax: (+91) 4027-160-921. E-mail: rkrana@iict.res.in.

Notes

The authors declare no competing financial interest.

■ ACKNOWLEDGMENTS

We acknowledge financial support from CSIR, India for SRF, IntelCoat (Grant CSC-0114), NanoSHE (Grant BSC-0112), and M2D (Grant CSC-0134).

■ REFERENCES

(1) Mclaren, A.; Valdes-Solis, T.; Li, G.; Tsang, S. C. Shape and Size Effects of ZnO Nanocrystals on Photocatalytic Activity. *J. Am. Chem. Soc.* **2009**, *131*, 12540–12541.

(2) Hoffmann, M. R.; Martin, S. T.; Choi, W.; Bahnemann, D. W. Environmental Applications of Semiconductor Photocatalysis. *Chem. Rev.* **1995**, *95*, 69–96.

(3) He, W.; Kim, H. K.; Wamer, W. G.; Melka, D.; Callahan, J. H.; Yin, J.-J. Photogenerated Charge Carriers and Reactive Oxygen Species in ZnO/Au Hybrid Nanostructures with Enhanced Photocatalytic and Antibacterial Activity. *J. Am. Chem. Soc.* **2014**, *136*, 750–757.

(4) Lee, J.; Shim, H. S.; Lee, M.; Song, J. K.; Lee, D. Size-Controlled Electron Transfer and Photocatalytic Activity of ZnO–Au Nanoparticle Composites. *J. Phys. Chem. Lett.* **2011**, *2*, 2840–2845.

(5) Zhang, Z.; Shao, C.; Li, X.; Zhang, L.; Xue, H.; Wang, C.; Liu, Y. Electrospun Nanofibers of ZnO-SnO_2 Heterojunction with High Photocatalytic Activity. *J. Phys. Chem. C* **2010**, *114*, 7920–7925.

(6) Sakthivel, S.; Geissen, S.-U.; Bahnemann, D. W.; Murugesan, V.; Vogelpohl, A. Enhancement of Photocatalytic Activity by Semiconductor Heterojunctions: α-Fe_2O_3, WO_3 and CdS Deposited on ZnO. *J. Photochem. Photobiol., A* **2002**, *148*, 283–293.

(7) Han, C.; Yang, M. Q.; Weng, B.; Xu, Y. J. Improving the Photocatalytic Activity and Anti-photocorrosion of Semiconductor ZnO by Coupling with Versatile Carbon. *Phys. Chem. Chem. Phys.* **2014**, *16*, 16891–16903.

(8) An, X.; Yu, J. C. Graphene-Based Photocatalytic Composites. *RSC Adv.* **2011**, *1*, 1426–1434.

(9) Xiang, Q.; Yu, J.; Jaroniec, M. Graphene-Based Semiconductor Photocatalysts. *Chem. Soc. Rev.* **2012**, *41*, 782–796.

(10) Zhang, L.; Cheng, H.; Zong, R.; Zhu, Y. Photocorrosion Suppression of ZnO Nanoparticles via Hybridization with Graphite-like Carbon and Enhanced Photocatalytic Activity. *J. Phys. Chem. C* **2009**, *113*, 2368–2374.

(11) Williams, G.; Kamat, P. V. Graphene-Semiconductor Nanocomposites: Excited-State Interactions between ZnO Nanoparticles and Graphene Oxide. *Langmuir* **2009**, *25*, 13869–13873.

(12) Wang, J.; Tsuzuki, T.; Tang, B.; Hou, X.; Sun, L.; Wang, X. Reduced Graphene Oxide/ZnO Composite: Reusable Adsorbent for Pollutant Management. *ACS Appl. Mater. Interfaces* **2012**, *4*, 3084–3090.

(13) Zou, R.; Zhang, Z.; Yu, L.; Tian, Q.; Chen, Z.; Hu, J. A General Approach for the Growth of Metal Oxide Nanorod Arrays on Graphene Sheets and Their Applications. *Chem. - Eur. J.* **2011**, *17*, 13912–13917.

(14) Feng, Y.; Feng, N.; Wei, Y.; Zhang, G. An *in situ* Gelatin-Assisted Hydrothermal Synthesis of ZnO–Reduced Graphene Oxide Composites with Enhanced Photocatalytic Performance Under Ultraviolet and Visible Light. *RSC Adv.* **2014**, *4*, 7933–7943.

(15) Li, X.; Wang, Q.; Zhao, Y.; Wu, W.; Chen, J.; Meng, H. Green Synthesis and Photo-catalytic Performances for ZnO-Reduced Graphene Oxide Nanocomposites. *J. Colloid Interface Sci.* **2013**, *411*, 69–75.

(16) Yang, Y.; Ren, L.; Zhang, C.; Huang, S.; Liu, T. Facile Fabrication of Functionalized Graphene Sheets (FGS)/ZnO Nanocomposites with Photocatalytic Property. *ACS Appl. Mater. Interfaces* **2011**, *3*, 2779–2785.

(17) Cao, X.; Zheng, B.; Rui, X.; Shi, W.; Yan, Q.; Zhang, H. Metal Oxide-Coated Three-Dimensional Graphene Prepared by the Use of Metal–Organic Frameworks as Precursors. *Angew. Chem., Int. Ed.* **2014**, *53*, 1404–1409.

(18) Qin, J.; Zhang, X.; Xue, Y.; Kittiwattanothai, N.; Kongsittikul, P.; Rodthongkum, N.; Limpanart, S.; Ma, M.; Liu, R. A Facile Synthesis of Nanorods of ZnO/Graphene Oxide Composites with Enhanced Photocatalytic Activity. *Appl. Surf. Sci.* **2014**, *321*, 226–232.

(19) Liu, X.; Pan, L.; Lv, T.; Lu, T.; Zhu, G.; Sun, Z.; Sun, C. Microwave-Assisted Synthesis of ZnO–Graphene Composite for Photocatalytic Reduction of Cr(VI). *Catal. Sci. Technol.* **2011**, *1*, 1189–1193.

(20) Luo, Q.-P.; Yu, X.-Y.; Lei, B.-X.; Chen, H.-Y.; Kuang, D.-B.; Su, C.-Y. Reduced Graphene Oxide-Hierarchical ZnO Hollow Sphere Composites with Enhanced Photocurrent and Photocatalytic Activity. *J. Phys. Chem. C* **2012**, *116*, 8111–8117.

(21) Chen, C. L.; Rosi, N. L. Peptide-Based Methods for the Preparation of Nanostructured Inorganic Materials. *Angew. Chem., Int. Ed.* **2010**, *49*, 1924–1942.

(22) Dickerson, M. B.; Sandhage, K. H.; Naik, R. R. Protein- and Peptide-Directed Syntheses of Inorganic Materials. *Chem. Rev.* **2008**, *108*, 4935–4978.

DOI: 10.1021/acsami.5b04820
ACS Appl. Mater. Interfaces 2015, 7, 19684–19690

(23) Begum, G.; Rana, R. K.; Singh, S.; Satyanarayana, L. Bioinspired Silicification of Functional Materials: Fluorescent Monodisperse Mesostructure Silica Nanospheres. *Chem. Mater.* **2010**, *22*, 551−556.
(24) Manna, J.; Rana, R. K. Oriented Morphogenesis of ZnO Nanostructures from Water-Soluble Zinc Salts under Environmentally Mild Conditions and Their Optical Properties. *Chem.−Eur. J.* **2012**, *18*, 498−506.
(25) Begum, G.; Manorama, S. V.; Singh, S.; Rana, R. K. Morphology-Controlled Assembly of ZnO Nanostructures: A Bioinspired Method and Visible Luminescence. *Chem.−Eur. J.* **2008**, *14*, 6421−6427.
(26) Park, S.; Dikin, D. A.; Nguyen, S. T.; Ruoff, R. S. Graphene Oxide Sheets Chemically Cross-Linked by Polyallylamine. *J. Phys. Chem. C* **2009**, *113*, 15801−15804.
(27) Kovtyukhova, N. I.; Ollivier, P. J.; Martin, B. R.; Mallouk, T. E.; Chizhik, S. A.; Buzaneva, E. V.; Gorchinskiy, A. D. Layer-by-Layer Assembly of Ultrathin Composite Films from Micron-Sized Graphite Oxide Sheets and Polycations. *Chem. Mater.* **1999**, *11*, 771−778.
(28) McAllister, M. J.; Li, J.-L.; Adamson, D. H.; Schniepp, H. C.; Abdala, A. A.; Liu, J.; Herrera-Alonso, M.; Milius, D. L.; Car, R.; Prud'homme, R. K.; Aksay, I. A. Single Sheet Functionalized Graphene by Oxidation and Thermal Expansion of Graphite. *Chem. Mater.* **2007**, *19*, 4396−4404.
(29) Chua, C. K.; Pumera, M. Chemical Reduction of Graphene Oxide: A Synthetic Chemistry Viewpoint. *Chem. Soc. Rev.* **2014**, *43*, 291−312.
(30) Zhang, S.; Shao, Y.; Liao, H.; Engelhard, M. H.; Yin, G.; Lin, Y. Polyelectrolyte-Induced Reduction of Exfoliated Graphite Oxide: A Facile Route to Synthesis of Soluble Graphene Nanosheets. *ACS Nano* **2011**, *5*, 1785−1791.
(31) Kumar, B.; Gong, H.; Chow, S. Y.; Tripathy, S.; Hua, Y. Photoluminescence and Multiphonon Resonant Raman Scattering in Low-Temperature Grown ZnO Nanostructures. *Appl. Phys. Lett.* **2006**, *89*, 071922−071923.
(32) Bai, X.; Wang, L.; Zong, R.; Lv, Y.; Sun, Y.; Zhu, Y. Performance Enhancement of ZnO Photocatalyst via Synergic Effect of Surface Oxygen Defect and Graphene Hybridization. *Langmuir* **2013**, *29*, 3097−3105.
(33) Compton, O. C.; Dikin, D. A.; Putz, K. W.; Brinson, L. C.; Nguyen, S. T. Electrically Conductive "Alkylated" Graphene Paper *via* Chemical Reduction of Amine-Functionalized Graphene Oxide Paper. *Adv. Mater.* **2010**, *22*, 892−896.
(34) Wang, J.; Wang, Z.; Huang, B.; Ma, Y.; Liu, Y.; Qin, X.; Zhang, X.; Dai, Y. Oxygen Vacancy Induced Band-Gap Narrowing and Enhanced Visible Light Photocatalytic Activity of ZnO. *ACS Appl. Mater. Interfaces* **2012**, *4*, 4024−4030.
(35) Zhang, X.; Qin, J.; Xue, Y.; Yu, P.; Zhang, B.; Wang, L.; Liu, R. Effect of Aspect Ratio and Surface Defects on The Photocatalytic Activity of ZnO Nanorods. *Sci. Rep.* **2014**, *4*, 4596.
(36) Li, Y. Z.; Xie, W.; Hu, X. L.; Shen, G. F.; Zhou, X.; Xiang, Y.; Zhao, X. J.; Fang, P. F. Comparison of Dye Photodegradation and Its Coupling With Light-to-Electricity Conversion Over TiO2 and ZnO. *Langmuir* **2010**, *26*, 591−597.
(37) Hummers, W. S.; Offeman, R. E. Preparation of Graphitic Oxide. *J. Am. Chem. Soc.* **1958**, *80*, 1339−1339.

DOI: 10.1021/acsami.5b04820
ACS Appl. Mater. Interfaces 2015, 7, 19684−19690